5038–5048 *Nucleic Acids Research, 2019, Vol. 47, No. 10* *Published online 27 March 2019*
doi: 10.1093/nar/gkz200

PRMT1 loss sensitizes cells to PRMT5 inhibition

Guozhen Gao[1,†], Liang Zhang[1,†], Oscar D. Villarreal[1], Wei He[1], Dan Su[2], Ella Bedford[1], Phoebe Moh[1], Jianjun Shen[1], Xiaobing Shi[3], Mark T. Bedford[1,*] and Han Xu[1,*]

[1]Department of Epigenetics and Molecular Carcinogenesis, The University of Texas MD Anderson Cancer Center, Smithville, TX 78957, USA, [2]Department of Experimental Radiation Oncology, The University of Texas MD Anderson Cancer Center, Houston, TX 77030, USA and [3]Center for Epigenetics, Van Andel Research Institute, Grand Rapids, MI 49503, USA

Received January 11, 2019; Revised February 22, 2019; Editorial Decision March 13, 2019; Accepted March 15, 2019

ABSTRACT

PRMT5 is an arginine methyltransferase that accounts for the vast majority of the symmetric methylation in cells. PRMT5 exerts its function when complexed with MEP50/WDR77. This activity is often elevated in cancer cells and correlates with poor prognosis, making PRMT5 a therapeutic target. To investigate the PRMT5 signaling pathway and to identify genes whose loss-of-function sensitizes cancer cells to PRMT5 inhibition, we performed a CRISPR/Cas9 genetic screen in the presence of a PRMT5 inhibitor. We identified known components of the PRMT5 writer/reader pathway including PRMT5 itself, MEP50/WDR77, PPP4C, SMNDC1 and SRSF3. Interestingly, loss of PRMT1, the major asymmetric arginine methyltransferase, also sensitizes cells to PRMT5 inhibition. We investigated the interplay between PRMT5 and PRMT1, and found that combinatorial inhibitor treatment of small cell lung cancer and pancreatic cancer cell models have a synergistic effect. Furthermore, *MTAP*-deleted cells, which harbor an attenuated PRMT5–MEP50 signaling pathway, are generally more sensitive to PRMT1 inhibition. Together, these findings demonstrate that there is a degree of redundancy between the PRMT5 and PRMT1 pathways, even though these two enzymes deposit different types of arginine methylation marks. Targeting this redundancy provides a vulnerability for tumors carrying a co-deletion of *MTAP* and the adjacent *CDKN2A* tumor suppressor gene.

INTRODUCTION

Arginine methylation is a prevalent post-translational modification, and roughly 0.5% of arginine residues are methylated in mouse and human cells (1,2). This modification has been implicated not only in many normal biological processes like transcription, splicing and signal transduction, but also in cancer (3). Arginine methylation is catalyzed by a group of nine protein arginine methyltransferases (PRMTs), which can be classified into three types: Type I (PRMT1, 2, 3, 4, 6 and 8) enzymes generate ω-N^G,N^G-asymmetric dimethylarginine (ADMA), Type II (PRMT5 and 9) enzymes generate ω-N^G,N'^G-symmetric dimethylarginine (SDMA) and the Type III (PRMT7) enzyme catalyzes the formation of ω-N^G-monomethyl arginine (MMA) residues in mammalian cells (4,5). PRMT1 is the primary Type I enzyme and PRMT5 is the primary Type II enzyme. PRMT1 functions largely on its own in cells, whereas PRMT5 is always complexed with the WD-repeat protein MEP50/WDR77 and is required for PRMT5 activity (6).

Both Type I and Type II PRMTs primarily methylate glycine- and arginine-rich motifs within their substrates (4,7). *In vitro* methylation experiments have demonstrated that a number of GAR motif-containing proteins are substrates for both PRMT1 and PRMT5, including Fibrillarin (8), CPSF6 and PABPN1 (9), and SMD3 (10). Also, specific arginine residues on non-GAR motif proteins, like the histone H4R3 site, are modified by both PRMT1 and PRMT5 (11–13). Furthermore, when PRMT1 is knocked out in MEFs, there is a rapid decrease in ADMA levels, concomitant with a dramatic increase in SDMA levels (1), which suggests that sites that were once methylated by PRMT1 are now available to PRMT5. Thus, it is clear that the same arginine residues can be marked symmetrically and asymmetrically depending on the local concentration of the PRMT.

Although arginine methylation does not alter the positive charge of the arginine residue, it does add steric bulk and bestow increased hydrophobicity (14), and these distinct features can promote molecular consequences, including: (i) the recognition by Tudor domain-containing proteins (15), or interference with protein–protein interactions that are driven by PHD fingers (16) and SH3 domains

*To whom correspondence should be addressed. Tel: +1 512 237 9539; Fax: +1 512 237 2475; Email: mtbedford@mdanderson.org
Correspondence may also be addressed to Han Xu. Tel: +1 512 237 9474; Fax: +1 512 237 2437; Email: hxu4@mdanderson.org
†The authors wish it to be known that, in their opinion, the first two authors should be regarded as Joint First Authors.

(17). SDMA motifs are recognized by the Tudor domain of SMN, SMNDC1/SPF30 and SND1, whereas ADMA marks are primarily 'read' by the Tudor domain of TDRD3 (18). (ii) Arginine methylation also affects the activity of certain kinases toward their substrates. Most notably, the consensus Akt phosphorylation motif harbors a critical arginine residue, which can be targeted for methylation by PRMTs. In the event of methylation, Akt-dependent phosphorylation of the adjacent serine residue is abrogated (19). (iii) Arginine methylation of GAR motifs has the propensity to regulate phase separation (20). Indeed, the RNA-binding protein FUS is a substrate for both PRMT1 and PRMT5 (21,22), and inhibition of methylation (using AdOx) of FUS promotes phase separation (23,24). Similarly, arginine methylation of hnRNPA2 also reduces its ability to phase separate (25). It is unclear if ADMA and SDMA marks play different roles in regulating phase separation.

To help elucidate the biological roles of the different PRMTs, genetic studies have leveraged mouse knockout models and biochemical studies have identified specific PRMT substrates and protein complexes (26). These efforts have been aided with the recent development of specific small molecule PRMT inhibitors (27), including very selective inhibitors to PRMT5 (28). Importantly, PRMT5 inhibition holds therapeutic promise for lymphomas and solid tumors, and is the first PRMT inhibitor to be tested in phase I clinical trials (29). There is also an emerging interest in targeting PRMT5 in methylthioadenosine phosphorylase (*MTAP*) null tumors (30–32). *MTAP* is frequently deleted in cancer due to its proximity to the commonly deleted tumor suppressor gene *CDKN2A*. These *MTAP*-null tumors have elevated levels of methylthioadenosine (MTA), which is the metabolite cleaved by MTAP, and MTA is a rather selective inhibitor of PRMT5. Thus, *MTAP*-null tumors have reduced levels of SDMA, as compared to the surrounding normal tissue.

Here, we used the PRMT5 inhibitor as a tool agent, in combination with a CRISPR/Cas9 genetic screen, to identify proteins that potentially reside in the PRMT5 pathway, or function synergistically with this pathway. We found PRMT1 to be a significant 'hit' in this screen, and we show that combining Type I (MS023) and Type II (EPZ015666) PRMT inhibitors has a synergistic effect on the growth of small cell lung cancer and pancreatic cancer cell line models. Related to this finding, we observe that *MTAP*-null cell lines are generally more sensitive to the Type I PRMT inhibitor compared with isogenic MTAP-expressing counterparts, likely due to the fact that the elevated MTA levels in these cells serve as a 'naturally' occurring inhibitor of PRMT5, which then synergizes with the Type I PRMT inhibitor.

MATERIALS AND METHODS

Cell lines and tissue culture

H2171, A549, MiaPaCa2, A172 and MCF-7 cells were originally purchased from ATCC. H2171 cells stably expressing inducible Cas9 (H2171-iCas9) were generated using lentivirus infection of a Doxycycline (Dox) responsive promoter driving Flag-tagged Cas9 (33) and subsequent Puromycin selection. Inducible PRMT1 knockout MEFs were obtained from Dr Stephan Richard. MTAP-rescued cell lines were made by infecting A549, MiaPaCa2, A172 and MCF-7 cells with lentivirus expressing MTAP under a CMV promoter, and were selected with Blasticidin S for 2 weeks. H2171 cells and H2171-iCas9 cells were cultured with HITES medium, supplemented with 5% FBS at 37°C with 5% CO_2. All other cells were cultured with DMEM medium, supplemented with 10% FBS at 37°C with 5% CO_2.

sgRNA library design

The sgRNA target sequences were selected based on SSC score (34) and the online tool CRISPR-FOCUS (35). Each oligo (75 nt) contains 19 nt sgRNA, 5′ universal flanking sequence: TATCTTGTGGAAAGGACGAAACACCg and 3′ universal flanking sequence: GTTTTAGAGCTAGAAA TAGCAAGTTAAAAT. The 'g' denotes an added G to the end of 5′ universal flanking sequence if the first nucleotide of guide sequence did not begin with a 'G'. This oligo library was synthesized as a pool by Custom Array Inc. (Bothell, WA). The sequences of sgRNAs are provided in Supplementary Table S1.

Oligo amplification, pooled library cloning and transformation

The oligo library was amplified using the following primer pair GGCTTTATATATCTTGTGGAA AGGACGAAACACCG (forward) and CTAGCCTTAT TTTAACTTGCTATTTCTAGCTCTAAAAC (reverse) using Phusion High-Fidelity PCR Master Mix (NEB, #M0531S) with four replicates, followed by purification (Qiagen, #28706). The purified product was cloned into the lentiviral sgRNA expression plasmid LentiGuide-Blast using Gibson Assembly Reaction Master Mix (NEB, #E2611S) as previously described with minor modifications (36). Briefly, Gibson ligation reaction was performed using 50 ng of the purified PCR product of oligo library and 450 ng BsmBI-digested LentiGuide-Blast with two replicates. Electrocompetent cells (25 μl, Lucigen, #60242) were transformed with 2 μl of the ligation product according to the manufacturer's protocol using a GenePulser (BioRad) and plated onto 15 cm plates with carbenicillin selection (50 μg/ml). To ensure no loss of representation, eight parallel transformations were performed, which should yield 200× library coverage. Colonies were scraped off plates, combined and used for plasmid DNA extraction with Endotoxin-Free Plasmid Maxiprep (Qiagen, #12362). LentiGuide-Blast plasmid was generated by swapping *Blasticidin* gene into lentiGuide-Puro (Addgene, #52963).

Lentivirus packaging of plasmid library and infection

To produce lentivirus, HEK293T cells were seeded into five 10-cm dishes at ∼40% confluence the day before transfection in fresh medium (DMEM supplemented with 10% FBS and 1% Penicillin–Streptomycin). Before transfection, 10 μg plasmid DNA (4 μg plasmid library: 4 μg psPAX2: 2 μg pMD2.G) was added into 500 μl pre-warmed Opti-MEM medium (Gibco, # 31985062), and then mixed with

24 μl X-tremeGene HP DNA Transfection Reagent (Roche, #6366236001) in 500 μl Opti-MEM medium. Thirty minutes after incubation at room temperature, the mixture was dropwise added into each 10-cm dish containing HEK293T cells. Virus supernatant was collected into a 50-ml tube 48 h after transfection, filtered through a 0.45-μm Acrodisc syringe filter, frozen in small volume and stored at −80°C until use. To determine multiplicity of infection (MOI), target cells in six-well plates with 5×10^6 cells/well were infected with different volumes of virus supplemented with 8 μg/ml polybrene (Millipore, #TR-1003-G) in fresh medium for 24 h, and then seeded into 15-cm dishes for Blasticidin (10 μg/ml) selection. Cell survival rate was tested by CellTiter-Glo assay (Promega, #G7572) until the rate was <5% in the untransfected population, and viral doses for different MOIs were calculated.

Pooled screening

H2171-iCas9 cells (a minimum of 2×10^7 cells with 5×10^6 cells/well in six-well plates per replicate) were infected with lentivirus of plasmid library at a low MOI of ≤0.3 as calculated above, and then selected with 10 μg/ml Blasticidin for 8 days. The resulting cells were collected and passaged at the density of ∼0.5×10^6 cells/ml in fresh medium and cultured for 5 days for recovery from selection stress. For PRMT5i screening, cells were cultured with PRMT5 inhibitor EPZ015666 at the concentration of 0.5 μM and 1 μg/ml Doxycycline to induce Cas9 expression. Cells cultured with Doxycycline and DMSO were used as the control. Medium was refreshed every 2–3 days and the cell density was kept at 1×10^6 cells/ml and cell number at a minimum of 500-fold coverage of the library (a representation of 500 cells per sgRNA) during each passaging until a defined time point. After 18 days of culture (10 population doublings), cells were collected for genomic DNA (gDNA) extraction using the Blood & Cell Culture Midi kit (Qiagen, #13343), according to the manufacturer's instructions.

The amplification and sequencing of sgRNA library were performed as previously described with minor modifications (36). The sgRNA inserts were amplified first by PCR using the primer pair, OuterF: GGACCCAGAGAGGGCCTATT and OuterR: AGTGGATCTCTGCTGTCCCT using PCR Master Mix (NEB, #M0541L) from 40 μg gDNA with 5 μg gDNA in each 100 μl reaction in order to achieve 500-fold coverage over the EpiC library. PCR products were purified (Qiagen, #28104) according to the manufacturer's instructions, and replicates were combined and then used for the second PCR to attach Illumina adaptors and barcodes. The second PCR was performed using 5 μl of the purified first PCR products and the primer pair, InnerF: CAAGCAGAAG ACGGCATACGAGATCXXXXXXTTTCTTGGGTA GTTTGCAGTTTT (XXXXXX represents the sample barcode) and InnerR: AATGATACGGCGACCACCGA GATCTACACCGACTCGGTGCCACTTTT. The primer sequences were provided in Supplementary Table S4. The second PCR products were purified by 1.5–2% agarose gel and purification kit (Qiagen, #28704). The resulting amplicons were quantified by Nanodrop and verified by agarose gel. Sequencing was performed on a NEXTSeq 500 (Illumina) using custom Illumina sequencing primer and indexing primer with a 75 bp single read run. Amplifications were carried out with 12 cycles for the first PCR and 16 cycles for the second PCR.

Data processing

The screen data were processed using MoPAC (Modular Pipeline for Analysis of CRISPR screens), a software tool for differential essentiality analysis of CRISPR-based functional screens. In brief, sequencing reads were aligned to the sgRNA library and were counted. The read count table was processed with a quality-control module, a rank-weighted average algorithm for gene essentiality measurement, a normalization module for removing biases caused by different depths of selection and the assessment of statistical significance based on normal distribution (Z-score). The MoPAC tool is publicly available at https://sourceforge.net/projects/mopac/.

PRMT inhibitor treatment

MS023 (Sigma, # SML1555) and EPZ015666 (Sigma, # SML1421) are dissolved in DMSO. Cells were treated with different concentrations of each compound or compounds combined for a total of 6 days in the synthetic lethality assay, and 8 days for the proliferation assay for the MTAP-rescued lines. Culture media were changed and new drugs were added every other day. DMSO was used for untreated control.

Cell proliferation assay and counting

The CellTiter-Glo luminescent kit (Promega) was used to measure the cell viability as well as the cell growth. Briefly, cells were incubated in opaque-walled multiwell plates. At the time of measuring, the pre-warmed reagent was directly added to the cell culture with 1:1 ratio in volume. The plates were shaken on a horizontal shaker at room temperature for 10 min and applied to a luminescence plate reader.

Antibodies and western blot analysis

The PRMT1 antibody was a generous gift from Dr Stephan Richard. Other antibodies used were anti-β-actin (Sigma #A1978), anti-MMA (Cell Signaling Technologies #8015), anti-SDMA (Cell Signaling Technologies #13222), anti-ADMA (Epicypher #13–0011 (Figure 2B) and Collaboration with Cell Signaling Technologies (Figure 4F)), anti-Smith Antigen (Y12 clone, Invitrogen #MA5–13449) and anti-MTAP (Cell Signaling Technologies #4158). Cell lysates were harvested and applied to western blotting. Briefly, cells were harvested, washed three times with phosphate-buffered saline (PBS) and then lysed with RIPA buffer (50 mM Tris–HCl, pH 7.5, 150 mM NaCl, 1% NP-40, 0.1% sodium dodecyl sulphate (SDS), 1% sodium deoxycholate, 5 mM ethylenediaminetetraacetic acid). Cell debris was discarded and SDS loading buffer was added to the supernatant. Protein samples were boiled for 5 min and loaded to sodium dodecylsulphate-polyacrylamide gel electrophoresis gel. Then, the proteins were electrophoresed

to separate and transferred to a Polyvinylidene difluoride (PVDF) membrane. The membrane was blocked with 5% fat-free milk for 1 h at room temperature and then incubated with primary antibodies at 4°C overnight. The membrane was then washed three times with PBST and incubated with secondary antibodies for 1 h at room temperature. After washing three times with PBST, the membrane was incubated with ECL reagent and the signals were detected on X-ray film.

RESULTS

A CRISPR/Cas9 genetic screen identifies PRMT1 dependency with PRMT5 inhibition

We hypothesize that some proteins, especially epigenetic regulators, function synergistically with PRMT5. In order to discover novel dependencies associated with PRMT5 inhibition, we searched for genetic vulnerabilities using a CRISPR screening approach. A potent and specific PRMT5 small molecule inhibitor (EPZ015666) was recently identified that facilitates this screen (28). We designed a barcode guide RNA (gRNA) library, named 'EpiC' for 'Epigenetic regulator CRISPR', which primarily targets epigenetic regulators and a list of major cancer regulators. The EpiC library harbors sgRNAs targeting 1016 epigenetic or cancer regulators in total. Ten sgRNAs were designed for each gene, which facilitated robust bioinformatic analysis. We also included sgRNAs that target 99 core-essential genes (990 sgRNAs, positive controls), 267 sgRNAs that target the AAVS 'safe harbor' locus and 797 non-targeting sgRNAs (negative controls) (Figure 1A and Supplementary Table S1).

The PRMT5 and MEP50 levels are elevated in multiple cancer types such as lung carcinomas and pancreatic ductal adenocarcinomas, and are associated with poor prognosis (Chen *et al.*). To identify a cancer cell model suitable for the screen, we analyzed publically available gene expression and shRNA screen datasets from Cancer Cell Line Encyclopedia (CCLE) and the DepMap project, respectively (37). We selected H2171, a small cell lung cancer model that is characterized by high PRMT5 mRNA expression but weak cellular dependency on PRMT5 (Supplementary Figure S1). This allowed a wide dynamic range of cell viability measurements in the screen. A stable Cas9-inducible (iCas9) H2171 cell line was generated and infected with the pooled lentiviral EpiC library. The infected H2171 cells were subjected to Doxycycline (Dox) induction and a 18-day selection under the treatment of EPZ015666 or DMSO (Figure 1B). At 0.5 μM EPZ015666 treatment, H2171 cells display a significant reduction of SDMA signal (Supplementary Figure S2) and we used this inhibitor concentration for the screen. The propensity for sgRNA loss or retention was then gauged by deep-sequencing of the sgRNA spacer sequence (Supplementary Table S2). We performed bioinformatics analysis using the Modular Pipeline for Analysis of CRISPR screens (MoPAC), a computational tool recently developed for differential essentiality analysis in high-throughput CRISPR-based functional screens. The quality-control analysis in MoPAC showed distinct signal distributions of positive and negative controls (Supplementary Figure S3), indicating robustness of cell viability measures in the experiment. With an FDR cut-off threshold set at 0.1, MoPAC identified seven genes whose loss sensitized the cells to EPZ015666 treatment in comparison to the DMSO condition (Figure 1C and Supplementary Table S3). We found the top ranked genes include PRMT5 itself. The increased sensitivity of PRMT5-loss cells to EPZ015666 is consistent with the dosage-sensitive PRMT5 dependency model proposed previously (30). We also identified other factors in the PRMT5 pathway, including (i) WDR77 (MEP50) that is the primary PRMT5 cofactor (38,39), (ii) SMNDC1 (SPF30) a Tudor domain-containing protein that 'reads' SDMA marks (40), (iii) PPP4C that is in a protein complex with SMN (41), which is also a major 'reader' of SDMA marks and (iv) the splicing factor SRSF3 that regulates alternative splicing in a similar manner to PRMT5 (42,43). In addition to these known players in the PRMT5 pathway, three novel epigenetic regulators were also top-listed, including HDGFRP2, PRMT1 and INO80B. The differential selection effects in the screen can also be visualized by direct comparison of the log2 fold-changes corresponding to multiple sgRNAs that target the PRMT1 and PRMT5 genes, suggesting high reproducibility (Figure 1D). Indeed, PRMT1 is thought largely to be in an independent pathway, but our data provides evidence for a degree of redundancy between PRMT1 and PRMT5. Moreover, PRMT1 is a cancer therapeutic target with potent inhibitors. Therefore, we further investigated the dependency of cells on PRMT1, when PRMT5 activity is reduced.

PRMT1 is the key Type I enzyme that displays a degree of redundancy with PRMT5

PRMT1 is the primary Type I PRMT, accounting for roughly 90% of global ADMA deposition (44). To confirm that PRMT1 loss sensitizes the cells to PRMT5 inhibition, we took advantage of PRMT1 inducible knockout MEFs, developed by the Richard group (45). We treated this MEF line with tamoxifen (4-OHT) to induce the deletion of *PRMT1* gene. Additionally, EPZ015666 was used to inhibit PRMT5 activity. Both PRMT1 knockout and PRMT5 inhibition led to suppression of cell proliferation to certain degree (Figure 2A). Using a Bliss independence model (46), we computed the expected combinatorial effect of PRMT1 knockout and PRMT5 inhibition, assuming no synergistic effect is present. The expected effect was then compared to the observed effect upon the combined treatment with Tamoxifen (PRMT1 loss) and EPZ015666. We found the combined treatment resulted in greater inhibition of cell proliferation than expectation, confirming the synergy between PRMT1 loss and PRMT5 inhibition. The effects of PRMT1 loss and PRMT5 inhibition on arginine methylation levels were confirmed by western analysis using methyl-specific antibodies (Figure 2B). These data suggest that PRMT5 and PRMT1 share certain cellular functions with regards to cell proliferation. Of note, loss of CARM1 (ranked 20th) or PRMT6 (ranked 55th) also sensitized cells to the PRMT5 inhibitor to a milder level in our screen (Supplementary Table S3), and all three of these PRMTs (PRMT1, CARM1 and PRMT6) may act through different mechanisms that all synergize with PRMT5. Thus, the Type I enzymes display a degree of redundancy with PRMT5, where PRMT1

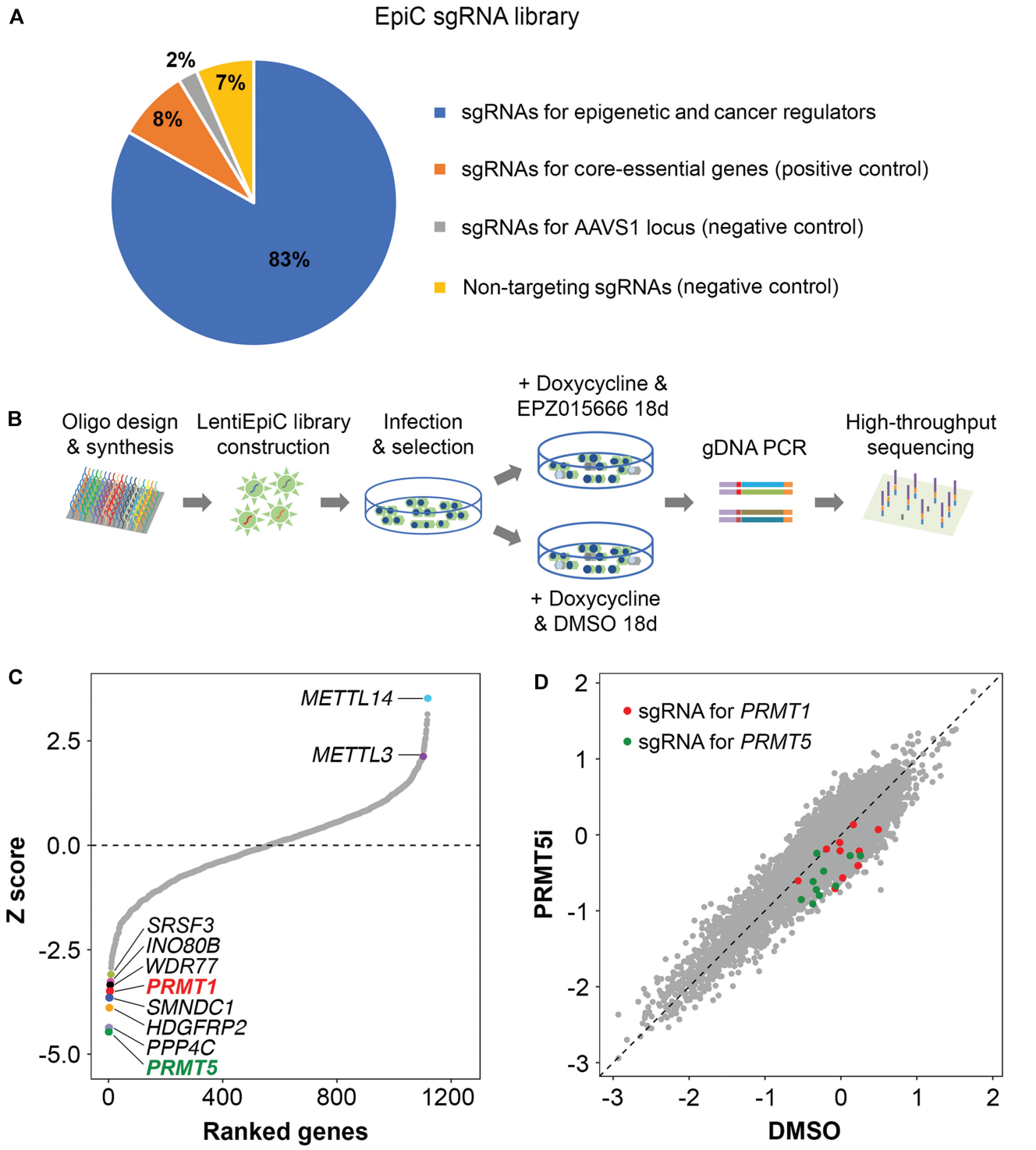

Figure 1. A CRISPR/Cas9 synthetic lethal screen with PRMT5 inhibitor EPZ015666 in H2171 cell line. (**A**) A pie chart showing the distribution of sgRNA composition in the EpiC library. (**B**) The workflow of the CRISPR/Cas9 screen. Pooled sgRNA oligos are cloned into LentiGuide-Blast plasmid and used for lentivirus packaging. After infection with the lentivirus, the iCas9 cell pool is subjected to Blasticidin selection. During screen, doxycycline (Dox, 1 μg/ml) was applied to induce Cas9-mediated knockout, and the cells were treated with PRMT5 inhibitor EPZ015666 (0.5 μM) or DMSO. Genomic DNA were harvested 18 days after Dox and EPZ015666/DMSO treatments. Nested PCR was performed to amplify sgRNA sequences, followed by next-generation sequencing. (**C**) All the 1016 genes in the EpiC library are ranked in order of *Z* scores, which measure the significance of essentiality changes with EPZ015666 treatment compared to the DMSO control. The top 7 genes with the most significant essentiality change (FDR < 0.1), as well as SRSF3 (FDR = 0.14, rank 8th), are highlighted. (**D**) The Log2 fold-change of sgRNA abundance in the PRMT5 inhibitor treatment versus DMSO control. The sgRNAs targeting PRMT1 and PRMT5 are highlighted.

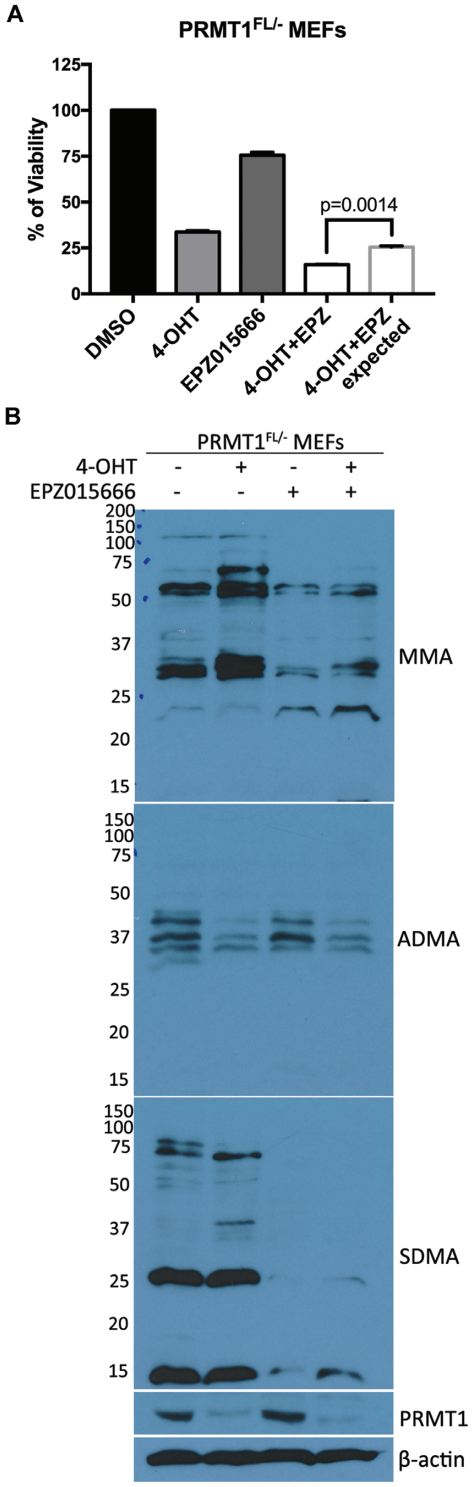

Figure 2. Validation of the synergistic effect of PRMT1-loss and PRMT5-loss using PRMT1 knockout MEF cells. PRMT1-inducible knockout MEF cells were treated with Tamoxifen (4-OHT), PRMT5 inhibitor or two chemicals combined for 6 days. 4-OHT treatment induced PRMT1 loss. (**A**) Cell viabilities under the treatments of DMSO, 4-OHT, EPZ015666, and the combination of 4-OHT and EPZ015666. Cell viability in each treated sample was measured using the CellTiter-Glo luminescence assay. The expected cell viability with 4-OHT+EPZ is computed using the Bliss Independence Model, which assumes no synergy. The *P*-value is based on paired *T*-test applied on three replicates. (**B**) The western blots showing the levels of MMA, ADMA, SDMA and PRMT1.

is the primary arginine methyltransferase to compensate for PRMT5 loss.

Dual inhibition of ADMA and SDMA production synergistically inhibits cell proliferation

To further investigate the potential synergistic effect of PRMT1 and PRMT5 loss on cell proliferation, we combined Type I (MS023) and Type II (EPZ015666) PRMT inhibitors, at different concentrations, on H2171 and MiaPaCa2, a pancreatic ductal carcinoma cell model (Figure 3A). We chose to test MiaPaCa2 as a second model because this cell line is distinct from H2171 cells in that it has lower levels of PRMT5 RNA expression and it is sensitive to PRMT5 knockdown (Supplementary Figure S1). MiaPaCa2 is also an MTAP-null line. The small molecule inhibitor MS023 is a rather general inhibitor of ADMA production in cells. It not only inhibits PRMT1 activity, but also inhibits the activity of PRMT3, CARM1, PRMT6 and PRMT8. As individual agents, 1–10 μM of EPZ015666 showed a mild inhibition of H2171 cell growth and a clear inhibition of MiaPaCa2 cell growth, while 1–10 μM of MS023 suppressed the proliferation rates of both cell lines. In a combinatorial setting, lower concentrations of MS023 and EPZ015666 (0.1–1 μM) inhibited the proliferation rates of both H2171 and MiaPaCa2 cells (Figure 3A), suggesting a synergistic effect.

We used two alternative methods, the combination index (CI) and the Bliss independence model, to evaluate synergism between MS023 and EPZ015666 in a quantitative manner (46). With a CI representation, both the 'effect-oriented' and 'dose-oriented' mapping of the data demonstrates synergism between MS023 and EPZ015666 (Figure 3B and C). Similarly, the Bliss independence model showed a synergistic effect >10% in both cell types, in a dosage range of 0.3 to 3.0 μM for MS023, and 0.1 to 1.0 μM for EPZ015666, respectively (Supplementary Figure S4A and B). Thus, in two different cell types, the combined loss of SDMA and ADMA has dramatic effects on cell proliferation rates and cell viability.

MTAP-deletion is associated with higher sensitivity to Type I PRMT inhibition

Recent studies have shown that *MTAP*-deleted cells are vulnerable to PRMT5 knockdown (30–32). This is due to the fact that *MTAP*-null cells have elevated levels of MTA, an analog of S-adenosylmethionine (AdoMet). MTA inhibits a large number of methyltransferases at high concentrations, but is 100-fold more selective against PRMT5 (IC_{50} = 3–5 μM). Thus, *MTAP*-null tumors (and cells) are likely to have reduced levels of SDMA, as compared to the surrounding normal tissue. Based on our findings above (Figures 2 and 3), we speculated that *MTAP*-null cells, which have attenuated SDMA levels, would be sensitive to the inhibition of Type I PRMTs by MS023.

To test this hypothesis, we took four known *MTAP*-null cell lines and rescued them to generate isogenic cell line pairs. These cell lines represent a spectrum of cancer types—A549 (lung carcinoma), MiaPaCa2 (pancreatic carcinoma), A172 (glioblastoma) and MCF7 (breast adeno-

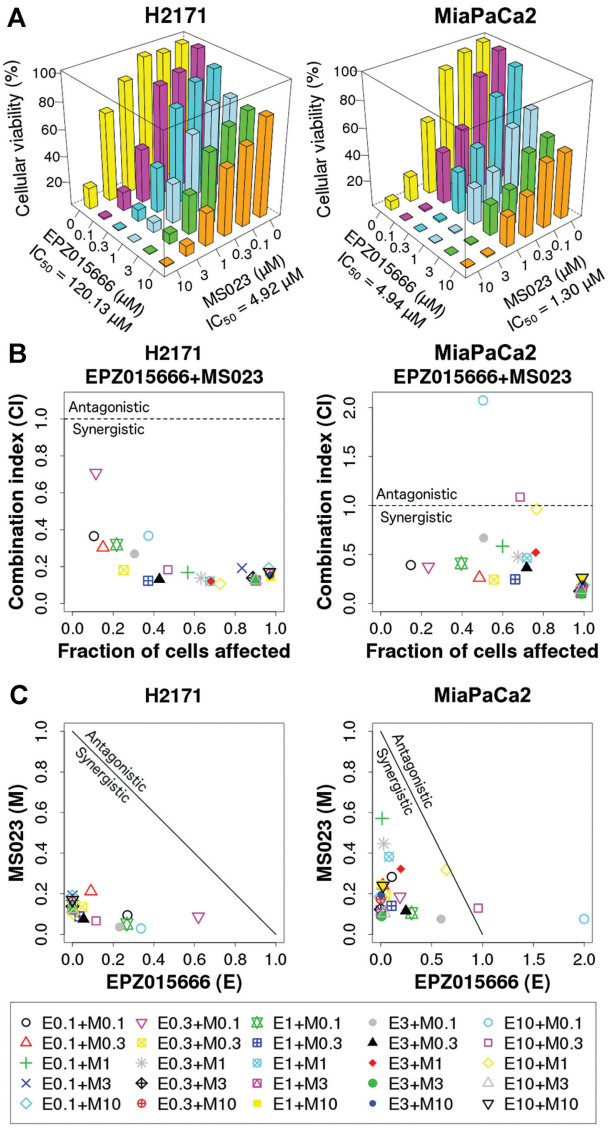

Figure 3. Synergistic interaction of SDMA and ADMA inhibition in the H2171 and MiaPaCa2 cell lines. (**A**) H2171 and MiaPaCa2 cells were treated with increasing concentrations of Type I (MS023) and Type II (EPZ015666) PRMT inhibitors, and analyzed for cellular viability. Compound treatment was performed for 6 days and the relative cell numbers (as a percentage of the untreated group) were counted. (**B**) The combination index (CI) values were calculated using CompuSyn software (ComboSyn, Inc., Paramus, NJ, USA) as a function of the fraction of cells affected (Chou-Talalay plot). Synergistic interactions are implied by values below 1, while values above 1 indicate antagonistic interactions. (**C**) Normalized isobolograms (Chou-Chou plots) corroborate the synergism for the indicated drug concentrations, the diagonal line corresponding to an additive effect. Combination data points falling on the lower left of this line indicate synergism, while those falling on the upper right indicate antagonism. The Key at the bottom represents the combination treatments used in μMs, with 'E' representing EPZ015666 and 'M' representing MS023.

carcinoma). All four cell lines displayed reduced proliferation in the presence of MS023 (Figure 4A–D, blue line). While rescuing of MTAP did not affect the cell proliferation when treated with DMSO control (Figure 4A–D, black and orange lines), three of the lines (A549, MiaPaCa2 and A172) were less sensitive to MS023 treatment (Figure 4A–D, pink line) when MTAP was rescued. Indeed, after 8 days of culture, in the presence of MS023, the three MTAP reconstituted cells displayed a 20% increase in cell number. In the case of MCF-7 cells, the reintroduction of MTAP had no effect on the sensitivity to MS023. These results suggest that a subset of *MTAP*-null cancer lines are more sensitive to Type I PRMT inhibition than their rescued counterparts.

To investigate possible phenotypes or behaviors that distinguish the MCF-7 cell line from the other three lines, we examined the *MTAP* copy number and PRMT5 dependency in 646 cancer cell lines from the DepMap project (37) (Figure 4E). By graphing PRMT5 knockdown against *MTAP* copy number, we clearly observe the vulnerability that was previously reported (30–32). Interestingly, approximately 15% of *MTAP*-null cell lines are insensitive to a reduction in PRMT5 levels by knockdown, including MCF-7. The other three lines we tested in this rescue experiment (A549, MiaPaCa2 and A172) were all sensitive to PRMT5 knockdown. Thus, the sensitivity to Type I PRMT inhibition is associated with cellular dependency on the PRMT5 pathway, confirming the synergy between PRMT1 and PRMT5 inhibitions.

Finally, we investigated the impact of MTAP rescue on the SDMA levels of these four cell lines. It has previously been shown that MTAP reconstituted lines display an increase in SDMA levels (30,32). This is consistent with the fact that the reintroduction of MTAP into these lines reduces MTA levels, and thus also alleviates the inhibition of PRMT5. We performed western analysis with the four rescued lines using a general anti-SDMA antibody, and the Y12 monoclonal antibody that recognizes symmetrically methylated SMB. We also observed the corresponding increase in SDMA levels (Figure 4F), but only in the lines that are sensitive to PRMT5 knockdown (Figure 4E) and responsive to MTAP rescue with regards to MS023 treatment (Figure 4A–D). Changes in SDMA levels are not observed in the rescued MCF-7 cell line. Taken together, *MTAP*-deletion is associated with higher dependency on PRMT1 in those cells that are sensitive to PRMT5 knockdown and display reduced SDMA levels upon MTAP loss.

DISCUSSION

The CRISPR screen identified multiple vulnerabilities in the presence of PRMT5 inhibition

Among the top hits in the screen were PRMT5 itself and WDR77 (MEP50), which is the critical PRMT5 cofactor (38,39), and the identification of these two genes provides internal validation of the screen. Furthermore, the identification of SMNDC1 (SPF30) also makes sense as it is a Tudor domain-containing protein that is a well-characterized 'reader' of SDMA marks, which are deposited by PRMT5 (40). The second highest ranked hit is PPP4C that is a serine/threonine phosphatase (47). PPP4C has been reported to interact with the SMN complex (41), and SMN is the major 'reader' of SDMA marks (48). Unfortunately, there has been no follow-up to determine how PPP4C potentially regulates the SMN complex. The EpiC sgRNA library did contain guides to both SMN1 and SMN2, but they were not 'hit' in the screen, likely due to the fact that these two proteins are identical in sequence and function

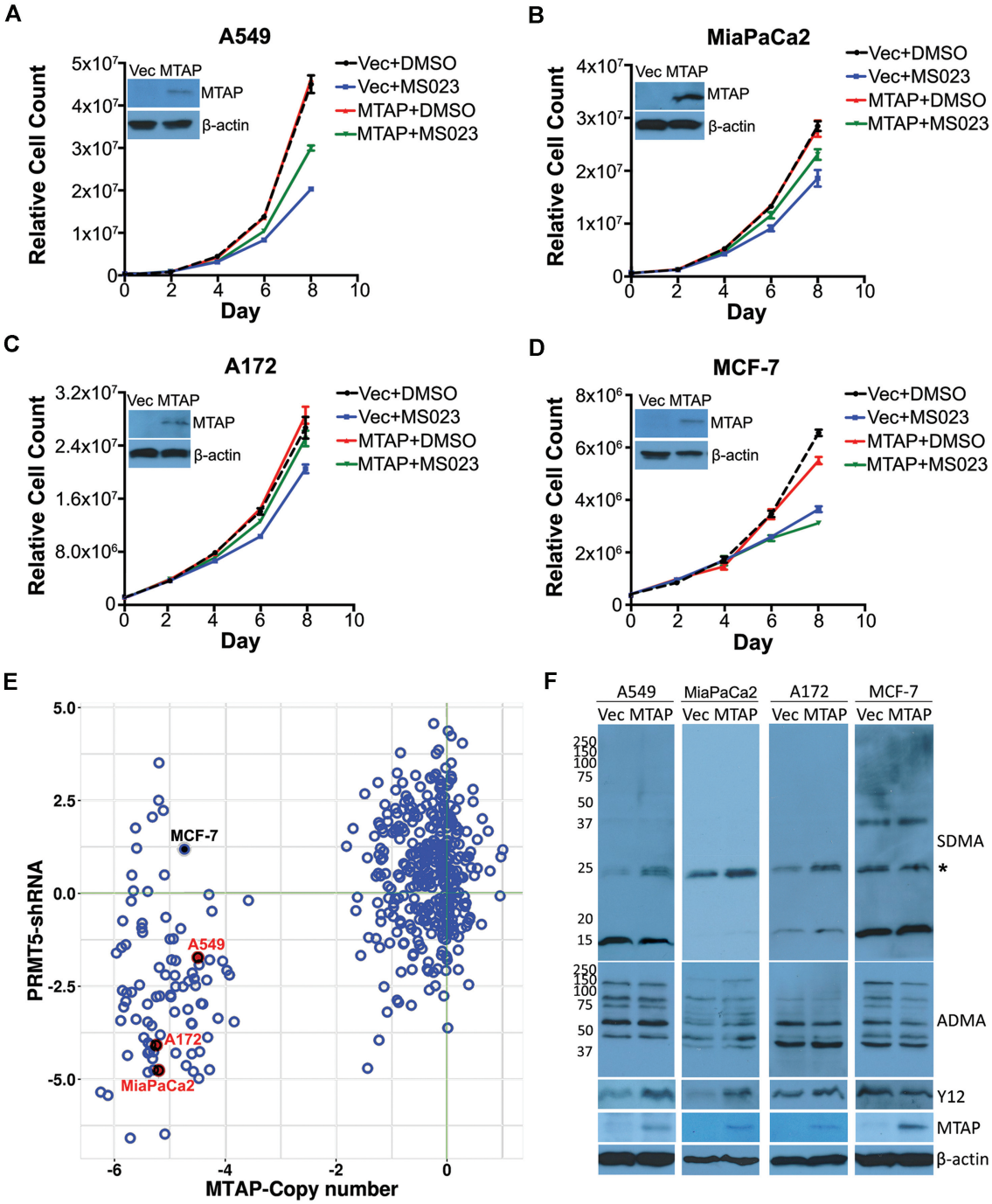

Figure 4. Different sensitivities of *MTAP*-deleted and MTAP-rescued cells to Type I PRMT inhibition. (**A–D**) *MTAP*-deleted cells were reconstituted with the stable re-expression of MTAP. These isogenic cell pairs were cultured for 8 days in the presence of DMSO or 1 μM of MS023 (0.1 μM for MiaPaCa2 cells). Different cell types display differing degrees of sensitivity to MS023, which we established empirically. The cell growth curves are plotted for A549 (A), MiaPaCa2 (B), A172 (C) and MCF-7 (D) cell lines. The expression levels of MTAP are shown for each pair of cell lines. (**E**) A scatter plot showing the sensitivities of *MTAP*-deleted cells to PRMT5 knockdown. Each dot in the scatter plot represents a cancer cell line. Data retrieved from the DepMap project (https://depmap.org/portal/). (**F**) Using total cell lysates from *MTAP*-deleted and MTAP-rescued cells, the levels of SDMA, ADMA, SmB methylation (Y12) and MTAP were analyzed by western blot.

redundantly in most tissues. It will be important to test the effects of a PPP4C inhibitor like Fortriecin on *MTAP*-null/reconstituted cell line pairs to further investigate the dependency of these cells on this phosphatase, through its ability to regulate the integrity of the SMN complex.

HDGFRP2 was also a highly ranked hit in our CRISPR screen (Figure 1C). The cellular functions of this protein remain largely unknown (49), although it has been implicated in the DNA repair pathway and homologous recombination (HR) (50). Hdgfrp2 knockout mice develop normally and are fertile (51), which suggests that only in the context of PRMT5 pathway attenuation is there for any cellular sensitivity to Hdgfrp2 loss. Interestingly, the HDGFRP2 protein harbors a PWWP domain that can bind methylated lysine residues (50), and it is possible that this domain could 'moonlight' as a SDMA-binding domain.

INO80B (ranked 7th) and INO80 (ranked 23rd) were also significant hits in this screen (Figure 1C and Supplementary Table S3). The INO80 complex facilitates ATP-dependent remodeling of chromatin and, like HDGFRP2, has been implicated in the regulation of HR (52). Importantly, PRMT5 was recently identified as a regulator of HR-mediated DNA repair through the TIP60/p400 complex (53). Thus, targeting of the HR pathway may also be a vulnerability for cells or tumors experiencing reduced PRMT5 activity. Another significant hit was SRSF3 (ranked 8th) (Supplementary Table S3), which is an oncogenic splicing factor. High levels of SRSF3 promote the inclusion of exon 6 of MDM4, which is required for a functional form of MDM4 that can target p53 for degradation (42). Similarly, PRMT5 is also critical for MDM4 exon 6 inclusion (43). PRMT5 and SRSF3 potentially regulate the same alternative splicing events, and it is thus not surprising to detect SRSF3 in this screen.

On the other end of the screen are the sgRNAs that are enriched in cells which display reduced sensitivity to PRMT5 inhibition. In a clinical setting, these hits may represent genes or pathways that could be lost to bestow resistance on this type of therapeutic intervention. Interestingly, the top hit is METTL14, which is an RNA methyltransferase that deposits the N6-methyladenosine (m^6A) mark (Figure 1C). The relevance of this hit is reinforced with the finding that sgRNAs that target METTL3 are also significantly enriched. METTL14 and METTL3 form a complex and both enzymes are required for optimal activity of the m6A methylosome (54).

What are the key shared substrates for PRMT1 and PRMT5?

The synergistic effects of PRMT1 and PRMT5 on cell proliferation imply that they may share common substrates that are regulated in the same way by both SDMA and ADMA marked motifs. Both PRMT1 and PRMT5 methylate RG/RGG motif-containing proteins (7), leading to a number of shared substrates that can be methylated by both PRMT1 and PRMT5. Indeed, histone H4 is methylated at the R3 site by both PRMT1 and PRMT5 (11,13), and was one of the first examples of the same residue being symmetrically methylated in two different ways. Other examples of common substrates include hnRNP A1 (55,56), Sam68, SLM-1, SLM-2 (57,58) and G3BP1 (59,60). These studies suggest a complicated crosstalk between PRMT1 and PRMT5 on many joint substrates, and it is unlikely that any one substrate will be responsible for the synergy seen between PRMT1 and PRMT5. Rather, the pleiotropic nature of this redundancy may be the driving force of the interdependency. It is also possible that the synergy we observe between PRMT1 and PRMT5 is not due to their redundant roles on common methylation sites, but rather because of their shared roles, through distinct substrates, in regulating major biological pathways like phase separation (20) and splicing (26).

Predicting sensitivity to Type I PRMT inhibitors in *MTAP*-null cells and tumors

It should be noted that PRMT1 was identified as a vulnerability in *MTAP*-deleted cells in the shRNA screen performed by the Marks group (32), and was ranked 12th, just after the PRMT5 cofactor RIOK1. However, it was not identified in the other two screens (30,31). Thus, it is perhaps not surprising that we identified PRMT1 in our CRISPR screen, in which PRMT5 activity was suppressed using a small molecule inhibitor instead of shRNA knockdown (Figure 1C and D). Therefore, it is likely that the synergy between PRMT1 and PRMT5 loss is dosage-dependent, where an inhibitor-based approach provides a higher quantitative resolution. We further show that when PRMT5 activity is suppressed due to elevated MTA levels (in *MTAP*-null cells), the cells are more sensitive to PRMT1 inhibition by MS023 in most cases, but not all (Figure 4A–D). The question is thus: Is it possible to predict which *MTAP*-null cell lines or tumors will be responsive to Type I PRMT inhibitor treatment? We tested four pairs of MTAP reconstituted lines, and found that the responsive lines (A549, MiaPaCa2 and A172) were all sensitive to PRMT5 knockdown (Figure 4E). The responsive lines also displayed lower SDMA levels in the absence of MTAP (Figure 4F). It is unclear what mechanism allows MCF-7 cells to escape sensitivity to PRMT5 knockdown or what accounts for the lack of SDMA change upon MTAP reconstituted. It could be increased PRMT5 activity in these cells, or reduced SDMA demethylase activity (if it does exist). The sensitivity of *MTAP*-null cell lines to PRMT5 knockdown could be used as an indicator for sensitivity to Type I PRMT inhibitors. This approach will not be of much use in predicting the responsiveness of *MTAP*-null tumors to this type of treatment in the future. However, immunohistochemical staining of tumor biopsies, using anti-SDMA antibodies, may be of predictive value.

SUPPLEMENTARY DATA

Supplementary Data are available at NAR Online.

ACKNOWLEDGEMENTS

Author Contributions: Guozhen Gao: Formal analysis related to PRMTs, investigation and writing. Liang Zhang: CRISPR library screen and investigation. Oscar D. Villarreal: Formal analysis and methodology development. Wei He: Formal analysis. Ella Bedford: CRISPR library

screen. Phoebe Moh: Methodology development. Dan Su: CRISPR library design and testing. Jianjun Shen: Deep-sequencing analysis. Xiaobing Shi: Conceptualization, CRISPR library design. Mark T. Bedford: Conceptualization, formal analysis and writing. Han Xu: Conceptualization, CRISPR library design, formal analysis and writing.

FUNDING

NIH [GM126421 to M.T.B., R25CA181004 in support of P.M.]; CPRIT [RR160097 to H.X., RP170002 to J.J.S.]. Funding for open access charge: CPRIT [RP170002].

Conflict of interest statement. M.T.B is a cofounder of EpiCypher. Other authors declare that they have no conflict of interest.

REFERENCES

1. Dhar,S., Vemulapalli,V., Patananan,A.N., Huang,G.L., Di Lorenzo,A., Comb,M.J., Guo,A., Clarke,S.G. and Bedford,M.T. (2013) Loss of the major Type I arginine methyltransferase PRMT1 causes substrate scavenging by other PRMTs. *Sci. Rep.*, **3**, 1311.
2. Paik,W.K. and Kim,S. (1980) *Natural Occurrence of Various Methylated Amino Acid Derivatives*. John Wiley & sons, NY.
3. Yang,Y. and Bedford,M.T. (2013) Protein arginine methyltransferases and cancer. *Nat. Rev. Cancer*, **13**, 37–50.
4. Bedford,M.T. and Clarke,S.G. (2009) Protein arginine methylation in mammals: who, what, and why. *Mol. Cell*, **33**, 1–13.
5. Yang,Y., Hadjikyriacou,A., Xia,Z., Gayatri,S., Kim,D., Zurita-Lopez,C., Kelly,R., Guo,A., Li,W., Clarke,S.G. *et al.* (2015) PRMT9 is a type II methyltransferase that methylates the splicing factor SAP145. *Nat. Commun.*, **6**, 6428.
6. Burgos,E.S., Wilczek,C., Onikubo,T., Bonanno,J.B., Jansong,J., Reimer,U. and Shechter,D. (2015) Histone H2A and H4 N-terminal tails are positioned by the MEP50 WD repeat protein for efficient methylation by the PRMT5 arginine methyltransferase. *J. Biol. Chem.*, **290**, 9674–9689.
7. Thandapani,P., O'Connor,T.R., Bailey,T.L. and Richard,S. (2013) Defining the RGG/RG motif. *Mol. Cell*, **50**, 613–623.
8. Cheng,D., Cote,J., Shaaban,S. and Bedford,M.T. (2007) The arginine methyltransferase CARM1 regulates the coupling of transcription and mRNA processing. *Mol. Cell*, **25**, 71–83.
9. Martin,G., Ostareck-Lederer,A., Chari,A., Neuenkirchen,N., Dettwiler,S., Blank,D., Ruegsegger,U., Fischer,U. and Keller,W. (2010) Arginine methylation in subunits of mammalian pre-mRNA cleavage factor I. *RNA*, **16**, 1646–1659.
10. Zurita-Lopez,C.I., Sandberg,T., Kelly,R. and Clarke,S.G. (2012) Human protein arginine methyltransferase 7 (PRMT7) is a type III enzyme forming omega-NG-monomethylated arginine residues. *J. Biol. Chem.*, **287**, 7859–7870.
11. Fabbrizio,E., El Messaoudi,S., Polanowska,J., Paul,C., Cook,J.R., Lee,J.H., Negre,V., Rousset,M., Pestka,S., Le Cam,A. *et al.* (2002) Negative regulation of transcription by the type II arginine methyltransferase PRMT5. *EMBO Rep.*, **3**, 641–645.
12. Strahl,B.D., Briggs,S.D., Brame,C.J., Caldwell,J.A., Koh,S.S., Ma,H., Cook,R.G., Shabanowitz,J., Hunt,D.F., Stallcup,M.R. *et al.* (2001) Methylation of histone H4 at arginine 3 occurs in vivo and is mediated by the nuclear receptor coactivator PRMT1. *Curr. Biol.*, **11**, 996–1000.
13. Wang,H., Huang,Z.Q., Xia,L., Feng,Q., Erdjument-Bromage,H., Strahl,B.D., Briggs,S.D., Allis,C.D., Wong,J., Tempst,P. *et al.* (2001) Methylation of histone H4 at arginine 3 facilitating transcriptional activation by nuclear hormone receptor. *Science*, **293**, 853–857.
14. Frankel,A. and Brown,J.I. (2018) Evaluation of kinetic data: What the numbers tell us about PRMTs. *Biochim. Biophys. Acta Proteins Proteom.*, **1867**, 306–316.
15. Lu,R. and Wang,G.G. (2013) Tudor: a versatile family of histone methylation 'readers'. *Trends Biochem. Sci.*, **38**, 546–555.
16. Iberg,A.N., Espejo,A., Cheng,D., Kim,D., Michaud-Levesque,J., Richard,S. and Bedford,M.T. (2008) Arginine methylation of the histone h3 tail impedes effector binding. *J. Biol. Chem.*, **283**, 3006–3010.
17. Bedford,M.T., Frankel,A., Yaffe,M.B., Clarke,S., Leder,P. and Richard,S. (2000) Arginine methylation inhibits the binding of proline-rich ligands to Src homology 3, but not WW, domains. *J. Biol. Chem.*, **275**, 16030–16036.
18. Liu,K., Guo,Y., Liu,H., Bian,C., Lam,R., Liu,Y., Mackenzie,F., Rojas,L.A., Reinberg,D., Bedford,M.T. *et al.* (2012) Crystal structure of TDRD3 and methyl-arginine binding characterization of TDRD3, SMN and SPF30. *PLoS One*, **7**, e30375.
19. Yamagata,K., Daitoku,H., Takahashi,Y., Namiki,K., Hisatake,K., Kako,K., Mukai,H., Kasuya,Y. and Fukamizu,A. (2008) Arginine methylation of FOXO transcription factors inhibits their phosphorylation by Akt. *Mol. Cell*, **32**, 221–231.
20. Chong,P.A., Vernon,R.M. and Forman-Kay,J.D. (2018) RGG/RG motif regions in RNA binding and phase separation. *J. Mol. Biol.*, **430**, 4650–4665.
21. Chitiprolu,M., Jagow,C., Tremblay,V., Bondy-Chorney,E., Paris,G., Savard,A., Palidwor,G., Barry,F.A., Zinman,L., Keith,J. *et al.* (2018) A complex of C9ORF72 and p62 uses arginine methylation to eliminate stress granules by autophagy. *Nat. Commun.*, **9**, 2794.
22. Tradewell,M.L., Yu,Z., Tibshirani,M., Boulanger,M.C., Durham,H.D. and Richard,S. (2012) Arginine methylation by PRMT1 regulates nuclear-cytoplasmic localization and toxicity of FUS/TLS harbouring ALS-linked mutations. *Hum. Mol. Genet.*, **21**, 136–149.
23. Hofweber,M., Hutten,S., Bourgeois,B., Spreitzer,E., Niedner-Boblenz,A., Schifferer,M., Ruepp,M.D., Simons,M., Niessing,D., Madl,T. *et al.* (2018) Phase separation of FUS is suppressed by its nuclear import receptor and arginine methylation. *Cell*, **173**, 706–719.
24. Qamar,S., Wang,G., Randle,S.J., Ruggeri,F.S., Varela,J.A., Lin,J.Q., Phillips,E.C., Miyashita,A., Williams,D., Strohl,F. *et al.* (2018) FUS phase separation is modulated by a molecular chaperone and methylation of arginine Cation-pi interactions. *Cell*, **173**, 720–734.
25. Ryan,V.H., Dignon,G.L., Zerze,G.H., Chabata,C.V., Silva,R., Conicella,A.E., Amaya,J., Burke,K.A., Mittal,J. and Fawzi,N.L. (2018) Mechanistic view of hnRNPA2 Low-Complexity domain structure, interactions, and phase separation altered by mutation and arginine methylation. *Mol. Cell*, **69**, 465–479.
26. Blanc,R.S. and Richard,S. (2017) Arginine methylation: the coming of age. *Mol. Cell*, **65**, 8–24.
27. Kaniskan,H.U. and Jin,J. (2017) Recent progress in developing selective inhibitors of protein methyltransferases. *Curr. Opin. Chem. Biol.*, **39**, 100–108.
28. Chan-Penebre,E., Kuplast,K.G., Majer,C.R., Boriack-Sjodin,P.A., Wigle,T.J., Johnston,L.D., Rioux,N., Munchhof,M.J., Jin,L., Jacques,S.L. *et al.* (2015) A selective inhibitor of PRMT5 with in vivo and in vitro potency in MCL models. *Nat. Chem. Biol.*, **11**, 432–437.
29. McCabe,M.T., Mohammad,H.P., Barbash,O. and Kruger,R.G. (2017) Targeting histone methylation in cancer. *Cancer J.*, **23**, 292–301.
30. Kryukov,G.V., Wilson,F.H., Ruth,J.R., Paulk,J., Tsherniak,A., Marlow,S.E., Vazquez,F., Weir,B.A., Fitzgerald,M.E., Tanaka,M. *et al.* (2016) MTAP deletion confers enhanced dependency on the PRMT5 arginine methyltransferase in cancer cells. *Science*, **351**, 1214–1218.
31. Mavrakis,K.J., McDonald,E.R. 3rd, Schlabach,M.R., Billy,E., Hoffman,G.R., deWeck,A., Ruddy,D.A., Venkatesan,K., Yu,J., McAllister,G. *et al.* (2016) Disordered methionine metabolism in MTAP/CDKN2A-deleted cancers leads to dependence on PRMT5. *Science*, **351**, 1208–1213.
32. Marjon,K., Cameron,M.J., Quang,P., Clasquin,M.F., Mandley,E., Kunii,K., McVay,M., Choe,S., Kernytsky,A., Gross,S. *et al.* (2016) MTAP deletions in cancer create vulnerability to targeting of the MAT2A/PRMT5/RIOK1 Axis. *Cell Rep.*, **15**, 574–587.
33. Wang,T., Wei,J.J., Sabatini,D.M. and Lander,E.S. (2014) Genetic screens in human cells using the CRISPR-Cas9 system. *Science*, **343**, 80–84.
34. Xu,H., Xiao,T., Chen,C.H., Li,W., Meyer,C.A., Wu,Q., Wu,D., Cong,L., Zhang,F., Liu,J.S. *et al.* (2015) Sequence determinants of improved CRISPR sgRNA design. *Genome Res.*, **25**, 1147–1157.

35. Cao,Q., Ma,J., Chen,C.H., Xu,H., Chen,Z., Li,W. and Liu,X.S. (2017) CRISPR-FOCUS: A web server for designing focused CRISPR screening experiments. *PLoS One*, **12**, e0184281.
36. Shalem,O., Sanjana,N.E., Hartenian,E., Shi,X., Scott,D.A., Mikkelson,T., Heckl,D., Ebert,B.L., Root,D.E., Doench,J.G. *et al.* (2014) Genome-scale CRISPR-Cas9 knockout screening in human cells. *Science*, **343**, 84–87.
37. Tsherniak,A., Vazquez,F., Montgomery,P.G., Weir,B.A., Kryukov,G., Cowley,G.S., Gill,S., Harrington,W.F., Pantel,S., Krill-Burger,J.M. *et al.* (2017) Defining a cancer dependency map. *Cell*, **170**, 564–576.
38. Antonysamy,S., Bonday,Z., Campbell,R.M., Doyle,B., Druzina,Z., Gheyi,T., Han,B., Jungheim,L.N., Qian,Y., Rauch,C. *et al.* (2012) Crystal structure of the human PRMT5:MEP50 complex. *Proc. Natl. Acad. Sci. USA*, **109**, 17960–17965.
39. Ho,M.C., Wilczek,C., Bonanno,J.B., Xing,L., Seznec,J., Matsui,T., Carter,L.G., Onikubo,T., Kumar,P.R., Chan,M.K. *et al.* (2013) Structure of the arginine methyltransferase PRMT5-MEP50 reveals a mechanism for substrate specificity. *PLoS One*, **8**, e57008.
40. Cote,J. and Richard,S. (2005) Tudor domains bind symmetrical dimethylated arginines. *J. Biol. Chem.*, **280**, 28476–28483.
41. Carnegie,G.K., Sleeman,J.E., Morrice,N., Hastie,C.J., Peggie,M.W., Philp,A., Lamond,A.I. and Cohen,P.T. (2003) Protein phosphatase 4 interacts with the Survival of Motor Neurons complex and enhances the temporal localisation of snRNPs. *J. Cell Sci.*, **116**, 1905–1913.
42. Dewaele,M., Tabaglio,T., Willekens,K., Bezzi,M., Teo,S.X., Low,D.H., Koh,C.M., Rambow,F., Fiers,M., Rogiers,A. *et al.* (2016) Antisense oligonucleotide-mediated MDM4 exon 6 skipping impairs tumor growth. *J. Clin. Invest.*, **126**, 68–84.
43. Bezzi,M., Teo,S.X., Muller,J., Mok,W.C., Sahu,S.K., Vardy,L.A., Bonday,Z.Q. and Guccione,E. (2013) Regulation of constitutive and alternative splicing by PRMT5 reveals a role for Mdm4 pre-mRNA in sensing defects in the spliceosomal machinery. *Genes Dev.*, **27**, 1903–1916.
44. Tang,J., Kao,P.N. and Herschman,H.R. (2000) Protein-arginine methyltransferase I, the predominant protein-arginine methyltransferase in cells, interacts with and is regulated by interleukin enhancer-binding factor 3. *J. Biol. Chem.*, **275**, 19866–19876.
45. Yu,Z., Chen,T., Hebert,J., Li,E. and Richard,S. (2009) A mouse PRMT1 null allele defines an essential role for arginine methylation in genome maintenance and cell proliferation. *Mol. Cell. Biol.*, **29**, 2982–2996.
46. Foucquier,J. and Guedj,M. (2015) Analysis of drug combinations: current methodological landscape. *Pharmacol. Res. Perspect.*, **3**, e00149.
47. Cohen,P.T., Philp,A. and Vazquez-Martin,C. (2005) Protein phosphatase 4–from obscurity to vital functions. *FEBS Lett.*, **579**, 3278–3286.
48. Friesen,W.J., Massenet,S., Paushkin,S., Wyce,A. and Dreyfuss,G. (2001) SMN, the product of the spinal muscular atrophy gene, binds preferentially to dimethylarginine-containing protein targets. *Mol. Cell*, **7**, 1111–1117.
49. Gao,K., Xu,C., Jin,X., Wumaier,R., Ma,J., Peng,J., Wang,Y., Tang,Y., Yu,L. and Zhang,P. (2015) HDGF-related protein-2 (HRP-2) acts as an oncogene to promote cell growth in hepatocellular carcinoma. *Biochem. Biophys. Res. Commun.*, **458**, 849–855.
50. Baude,A., Aaes,T.L., Zhai,B., Al-Nakouzi,N., Oo,H.Z., Daugaard,M., Rohde,M. and Jaattela,M. (2016) Hepatoma-derived growth factor-related protein 2 promotes DNA repair by homologous recombination. *Nucleic Acids Res.*, **44**, 2214–2226.
51. Wang,H., Shun,M.C., Dickson,A.K. and Engelman,A.N. (2015) Embryonic lethality due to arrested cardiac development in Psip1/Hdgfrp2 Double-Deficient mice. *PLoS One*, **10**, e0137797.
52. Alatwi,H.E. and Downs,J.A. (2015) Removal of H2A.Z by INO80 promotes homologous recombination. *EMBO Rep.*, **16**, 986–994.
53. Clarke,T.L., Sanchez-Bailon,M.P., Chiang,K., Reynolds,J.J., Herrero-Ruiz,J., Bandeiras,T.M., Matias,P.M., Maslen,S.L., Skehel,J.M., Stewart,G.S. *et al.* (2017) PRMT5-Dependent methylation of the TIP60 Coactivator RUVBL1 is a key regulator of homologous recombination. *Mol. Cell*, **65**, 900–916.
54. Balacco,D.L. and Soller,M. (2019) The m(6)A Writer: Rise of a machine for growing tasks. *Biochemistry*, **58**, 363–378.
55. Wall,M.L. and Lewis,S.M. (2017) Methylarginines within the RGG-Motif region of hnRNP A1 affect its IRES Trans-Acting factor activity and are required for hnRNP A1 stress granule localization and formation. *J. Mol. Biol.*, **429**, 295–307.
56. Gao,G., Dhar,S. and Bedford,M.T. (2017) PRMT5 regulates IRES-dependent translation via methylation of hnRNP A1. *Nucleic Acids Res.*, **45**, 4359–4369.
57. Cote,J., Boisvert,F.M., Boulanger,M.C., Bedford,M.T. and Richard,S. (2003) Sam68 RNA binding protein is an in vivo substrate for protein arginine N-methyltransferase 1. *Mol. Biol. Cell*, **14**, 274–287.
58. Rho,J., Choi,S., Jung,C.R. and Im,D.S. (2007) Arginine methylation of Sam68 and SLM proteins negatively regulates their poly(U) RNA binding activity. *Arch. Biochem. Biophys.*, **466**, 49–57.
59. Bikkavilli,R.K. and Malbon,C.C. (2011) Arginine methylation of G3BP1 in response to Wnt3a regulates beta-catenin mRNA. *J. Cell Sci.*, **124**, 2310–2320.
60. Tsai,W.C., Gayatri,S., Reineke,L.C., Sbardella,G., Bedford,M.T. and Lloyd,R.E. (2016) Arginine demethylation of G3BP1 promotes stress granule assembly. *J. Biol. Chem.*, **291**, 22671–22685.